Biallelic truncating mutations in *ALPK3* cause severe pediatric cardiomyopathy

Rowida Almomani*, Judith M.A. Verhagen*, Johanna C. Herkert, Erwin Brosens, Karin Y. van Spaendonck-Zwarts, Angeliki Asimaki, Paul A. van der Zwaag, Ingrid M.E. Frohn-Mulder, Aida M. Bertoli-Avella, Ludolf G. Boven, Marjon A. van Slegtenhorst, Jasper J. van der Smagt, Wilfred F.J. van IJcken, Bert Timmer, Margriet van Stuijvenberg, Rob M. Verdijk, Jeffrey E. Saffitz, Frederik A. du Plessis, Michelle Michels, Robert M.W. Hofstra, Richard J. Sinke, J. Peter van Tintelen, Marja W. Wessels, Jan D.H. Jongbloed*, Ingrid M.B.H. van de Laar*

**These authors contributed equally*

Journal of the American College of Cardiology 2016;67(5):515-25

Abstract

Background

Cardiomyopathies represent a heterogeneous group of disorders characterized by structural and functional abnormalities of the myocardium and are associated with significant morbidity and mortality. The condition is usually inherited and predominantly affects adults, but can also present in childhood. Our understanding of the molecular basis of pediatric cardiomyopathy has improved significantly over the last two decades. However, the underlying mechanism remains elusive in a substantial proportion of cases. This study aimed to identify new genes involved in pediatric cardiomyopathy.

Methods

We performed homozygosity mapping and whole exome sequencing in two consanguineous families with idiopathic pediatric cardiomyopathy. Sixty unrelated patients with pediatric cardiomyopathy were subsequently screened for mutations in a candidate gene. First-degree relatives were submitted to cardiac screening and cascade genetic testing. Myocardial samples from two patients were processed for histological and immunohistochemical studies.

Results

We identified five patients from three unrelated families with pediatric cardiomyopathy caused by homozygous truncating mutations (c.4736-1G>A [p.Val1579Glyfs*30], c.3781C>T [p.Arg1261*] and c.5294G>A [p.Trp1765*]) in *ALPK3*, a gene encoding a nuclear kinase that plays an essential role in early differentiation of cardiomyocytes. All patients with biallelic mutations presented with severe hypertrophic and/or dilated cardiomyopathy in utero, at birth or in early childhood. Three patients died from heart failure within the first week of life. Moreover, two out of ten (20%) heterozygous family members showed hypertrophic cardiomyopathy with an atypical distribution of hypertrophy. Deficiency of alpha-kinase 3 has previously been associated with features of both hypertrophic and dilated cardiomyopathy in mice. Consistent with studies in knockout mice, we provide microscopic evidence for intercalated disc remodeling.

Conclusions

Biallelic truncating mutations in the newly identified gene *ALPK3* give rise to severe, early-onset cardiomyopathy in humans. Our findings highlight the importance of transcription factor pathways in the molecular mechanisms underlying human cardiomyopathies.

Introduction

Cardiomyopathies represent a clinically and genetically heterogeneous group of disorders affecting the ventricular myocardium. Among children aged < 18 years, the overall incidence of cardiomyopathy is 1.13 cases per 100,000 annually in the United States [1]. Pediatric cardiomyopathy is associated with significant morbidity and mortality: up to 40% of affected children die or undergo cardiac transplantation within five years of diagnosis [2, 3]. Cardiomyopathy can be classified into five clinical phenotypes based upon morphological and functional characteristics: hypertrophic cardiomyopathy (HCM), dilated cardiomyopathy (DCM), restrictive cardiomyopathy (RCM), arrhythmogenic right ventricular cardiomyopathy (ARVC), and unclassified cardiomyopathy, including left ventricular noncompaction (LVNC) [4]. The etiology of cardiomyopathy is extremely diverse, particularly in the pediatric population, and encompasses both non-genetic and genetic causes, including myocarditis, neuromuscular diseases, inborn errors of metabolism, malformation syndromes and familial forms caused by mutations in genes encoding the specialized, often structural, components of cardiomyocytes. Since the routine incorporation of genetic testing in the diagnostic evaluation of patients with cardiomyopathy, a causal diagnosis can be identified in more than 70% of children [5]. Interestingly, the same genetic causes that result in cardiomyopathy in adults are prevalent in the pediatric population (e.g. sarcomeric or cytoskeletal gene mutations) [6]. Despite recent advances in understanding the genetic etiologies of pediatric cardiomyopathy, a substantial number of cases remain unsolved, suggesting that other genes await discovery. Establishing an underlying genetic cause for cardiomyopathy allows presymptomatic identification of family members at risk and facilitates reproductive decision-making. Genetic and genomic studies continue to provide new insights into the pathophysiologic processes contributing to cardiomyopathy and will ultimately facilitate the development of patient-specific prevention and treatment strategies.

In order to identify new genes contributing to pediatric cardiomyopathy, we employed a combined approach of homozygosity mapping and whole exome sequencing in two consanguineous families with early-onset cardiomyopathy.

Methods

Patient population

We studied four individuals with pediatric cardiomyopathy from two consanguineous families of Dutch and Moroccan descent, respectively (**Figures 1A** and **1B**). A third family of Turkish descent was identified by subsequent cohort screening (**Figure 1C**). Patients underwent extensive clinical investigations including high-resolution prenatal ultrasound, physical examina-

tion, 12-lead electrocardiography, transthoracic echocardiography and post-mortem examination. Mutation screening of up to 48 known cardiomyopathy-related genes per individual was negative. A complete overview of the genetic and metabolic tests performed prior to this study is provided online (Detailed Methods, **Supplemental Information**). All asymptomatic siblings and parents underwent echocardiographic screening. HCM was defined by the presence of increased left ventricular (LV) wall thickness (>2 SD above the mean for body surface area in children or ≥13 mm in adult relatives) in the absence of hemodynamic stresses sufficient to account for the degree of hypertrophy. DCM was defined by the presence of LV dilatation (LV end-diastolic dimension (LVEDD) >2 SD above the mean for body surface area) and systolic dysfunction (fractional shortening (FS) or LV ejection fraction (EF) >2 SD below the mean for age) in the absence of abnormal loading conditions sufficient to cause global systolic impairment [4]. A cohort of 60 unrelated patients with idiopathic pediatric cardiomyopathy from diverse ethnic backgrounds was available for mutational screening of candidate genes. These patients had previously been screened for mutations in known cardiomyopathy-related genes (ranging from 8 to 55 genes). The Medical Ethical Committees of the University Medical Center Groningen and the Erasmus University Medical Center approved this study. Written informed consent was obtained from all participants or their legal guardians.

Homozygosity mapping

Genomic DNA was extracted from peripheral blood samples (A-VIII:1, VIII:2, IX:1 and IX:2; B-III:1, IV:3 and IV:4), buccal swabs (A-IX:3 and IX:4), amniotic fluid (B-IV:1) or fibroblasts (B-IV:2) (**Figure 1**). Genome-wide genotyping was performed using the Human610-Quad BeadChip (family A) or HumanCytoSNP-12 v2.1 BeadChip (family B) SNP array according to the manufacturer's instructions (Illumina, San Diego, CA, USA). Raw data were normalized and converted into genotypes using the GenomeStudio data analysis software. Genotype files were uploaded into the web-based tool HomozygosityMapper in order to detect homozygous stretches (>5 Mb) in the patients that were not present in their unaffected relatives [7].

Whole exome sequencing

Genomic DNA was sheared by sonication (Covaris, Woburn, MA, USA). Size distribution of fragmented DNA was analyzed on an Agilent 2100 Bioanalyzer System using the DNA 1000 kit. Targets were captured with the SureSelect Human All Exon 50 Mb kit V4 (Agilent Technologies, Santa Clara, CA, USA). Paired-end sequencing (2x101 bp) was performed on an Illumina Hiseq2000 platform (Illumina, San Diego, CA, USA). The sequence reads were mapped and aligned against the human reference genome GRCh37/hg19 with the Burrows-Wheeler Aligner [8]. Variant calling was performed using the Genome Analysis Toolkit (GATK) and SAMtools [9, 10]. Variant filtering was performed using Cartagenia Bench Lab NGS version 4.02 (Cartagenia, Leuven, Belgium). Variants were filtered on quality (read depth ≥6) and location (within an exon or first/last 20 bp of introns). Variants with a minor allele frequency (MAF) ≥

1% in at least 200 chromosomes in dbSNP, the Genome of the Netherlands [11], the 1000 Genomes Project [12] or an in-house reference set, or a MAF ≥ 3% in the NHLBI Go Exome Sequencing Project (ESP) were excluded from further analysis. Assuming an autosomal recessive model of inheritance, we selected variants found in heterozygous state in the father and in homozygous state in the patient. Only variants predicted to change the protein sequence (non-synonymous single nucleotide variants and short insertions and deletions) or the recognition of consensus RNA splice sites were considered. Finally, we filtered for variants present in the homozygous regions.

Sanger sequencing

Bidirectional Sanger sequencing of the entire coding region and exon-intron boundaries of the alpha-kinase 3 gene (*ALPK3*) was performed using polymerase chain reaction (PCR) primers designed by Primer3 software (http://bioinfo.ut.ee/primer3/) (**Supplemental Table 1**). PCR amplification was performed using the AmpliTaq Gold 360 Master Mix (Invitrogen, Life Technologies, Carlsbad, CA, USA) following the manufacturer's protocol. PCR fragments were purified with ExoSAP-IT (Affymetrix, Santa Clara, CA, USA) and subsequently sequenced on an ABI3730xl DNA Analyzer using BigDye Terminator v3.1 (Applied Biosystems, Foster City, CA, USA). Analysis of sequence data was performed using Mutation Surveyor (SoftGenetics, State College, PA, USA) and SeqScape v2.5 software (Applied Biosystems). For annotation of DNA and protein changes, the mutation nomenclature recommendations from the Human Genome Variation Society were followed [13]. Nucleotide numbering reflects cDNA numbering with +1 corresponding to the adenine (A) of the ATG translation initiation codon in the reference sequence NM_020778.4.

In silico analysis of variants

To assess the effect of the sequence variants identified on protein structure and function, we used prediction programs integrated in the Alamut Visual v2.6.1 software (Interactive Biosoftware, Rouen, France), including Polymorphism Phenotyping v2 (PolyPhen-2), Sorting Intolerant From Tolerant (SIFT) and MutationTaster [14-16]. Furthermore, possible effects on splicing were predicted using the integrated algorithm tools SpliceSiteFinder-like, MaxEntScan, Splice Site Prediction by Neural Network, GeneSplicer and Human Splicing Finder.

Reverse transcriptase PCR product analysis

To investigate the effect of the splice site variant c.4736-1G>A at the RNA level, we performed reverse transcriptase PCR analysis (RT-PCR) on RNA isolated from fibroblasts of the affected individual (A-IX:2) and two age-matched controls. Cells were cultured in Dulbecco's Modified Eagle Medium supplemented with 10% fetal bovine serum, 1% penicillin/streptomycin, 1% glucose, and 1% glutamax, in atmospheric oxygen and 5% CO_2 at 37°C. Total RNA was extracted with the RNeasy Mini Kit from QIAGEN. RT-PCR was performed using gene-specific

primers designed to amplify the exon expected to be affected by the mutation and flanking sequences (**Supplemental Figure 1**). The resulting PCR products were examined by 2% agarose gel electrophoresis and subsequently subjected to Sanger sequencing.

Histology

Paraffin-embedded or frozen cardiac tissue was available from two affected individuals (A-IX:2 and B-IV:2). Muscle biopsy specimens from the lateral portion of the quadriceps femoris muscle were available from another affected individual (B-IV:3) and her healthy sister (B-IV:4). Tissues from age-matched donors were used as controls. All samples were histologically examined after hematoxylin and eosin (H&E) and desmin staining using standard techniques.

Immunohistochemistry

Immunohistochemical analysis was performed on myocardial samples from individual A-IX:2 and two age-matched controls with no clinical or pathological evidence of heart disease, as described previously [17]. In brief, glass-mounted sections of formalin-fixed, paraffin-embedded myocardium (5 µm) were deparaffinized and rehydrated before antibody retrieval. Primary antibodies included mouse monoclonal anti-plakoglobin (Sigma-Aldrich, 1:1000 dilution), mouse monoclonal anti-plakophilin2 (2a+2b, Fitzgerald, undiluted), mouse monoclonal anti-desmoplakin (Fitzgerald, 1:10 dilution), mouse monoclonal anti–pan cadherin (Sigma-Aldrich, 1:400 dilution), rabbit polyclonal anti-43 (Sigma-Aldrich, 1:400 dilution) and rabbit polyclonal anti-desmin (Abcam, 1:100 dilution). The slides were then incubated with indocarbocyanine-conjugated goat anti–mouse or goat anti–rabbit secondary antibodies (Jackson Immunolabs; 1:400 dilution). Immunostained preparations were analyzed by laser scanning confocal microscopy.

Results

Clinical description

Results are summarized in **Table 1**.

Family A: The second child of healthy Dutch parents was born at 35 weeks following an uneventful pregnancy (IX:2; **Figure 1A**). At birth he presented with respiratory insufficiency and cyanosis. Echocardiography showed severe dilatation of the left ventricle (LVEDD 23.5 mm; z-score unreliable because of massive edema) with markedly reduced contractility of both ventricles and mitral and tricuspid regurgitation. He died due to progressive heart failure at the age of five days. Parents agreed on autopsy (see Histology section). Genealogical evaluation revealed that the parents were sixth degree cousins. Family history was negative for sudden death or cardiomyopathies. Echocardiography revealed no abnormalities in his parents (aged 34 and 31 years), his two brothers (aged 9 and 6 years) and his sister (aged 7 years).

Table 1. Clinical features of the affected individuals with *ALPK3* mutations

Individual	Sex	Origin	Age at diagnosis	Presenting symptoms	Outcome	Genotype
A-IX:2	M	Dutch	at birth	severe biventricular dilatation	d. 5 days postpartum	homozygous c.4736-1G>A, p.(Val1579Glyfs*30)
B-IV:1	F	Moroccan	33 weeks gestation	generalized hydrops fetalis, cardiomegaly	d. 36 weeks gestation	homozygous c.3781C>T, p.(Arg1261*)
B-IV:2	F	Moroccan	20 weeks gestation	generalized hydrops fetalis, severe biventricular hypertrophy and dilatation, severe tricuspid regurgitation	d. 2 hours postpartum	homozygous c.3781C>T, p.(Arg1261*)
B-IV:3	F	Moroccan	at birth	severe concentric LV hypertrophy	status quo (11 years)	homozygous c.3781C>T, p.(Arg1261*)
C-IV:1	M	Turkish	29 years	asymmetrical septum hypertrophy, RV hypertrophy	status quo (45 years)	heterozygous c.5294G>A, p.(Trp1765*)
C-IV:2	M	Turkish	27 years	concentric LV hypertrophy with relative sparing of basal segments, RV hypertrophy	status quo (43 years)	heterozygous c.5294G>A, p.(Trp1765*)
C-V:2	M	Turkish	4 years	severe concentric LV hypertrophy, RV hypertrophy	ventricular fibrillation, ICD implantation (7 years)	homozygous c.5294G>A, p.(Trp1765*)

ICD, implantable cardioverter defibrillator; LV, left ventricle; RV, right ventricle.

Family B: In the first pregnancy of healthy consanguineous Moroccan parents (IV:1; **Figure 1B**), prenatal ultrasound examination at 33 weeks of gestation revealed generalized hydrops fetalis and cardiomegaly with reduced contractility. The pregnancy ended in intrauterine fetal death at 35 weeks. External examination of the fetus did not show any gross abnormalities except massive skin edema. Autopsy was declined by the parents. The second pregnancy resulted in a spontaneous abortion. During the third pregnancy, ultrasound examinations at 20 and 26 weeks of gestation showed an enlarged heart with severely reduced contractility, a thickened myocardium with spongy appearance and severe tricuspid regurgitation (**Figure 2A**). At 30 weeks of gestation, severe fetal hydrops had developed. The patient was born at 36 weeks (IV:2; **Figure 1B**) and presented with severe respiratory distress. Echocardiography revealed severe hypertrophy and dilatation of both ventricles. She died two hours postpartum. Her parents agreed to a detailed post-mortem examination of the heart (see Histology section). In the fourth dizygotic twin pregnancy, extensive prenatal ultrasounds revealed no abnormalities. The twin girls were born at 37 weeks. Echocardiography at day 4 showed severe concentric HCM in one of the twins (IV:3; **Figure 1B**) which remained stable over subsequent years. Cardiac examination in patient IV:3 at age 10 years showed increased thickness of the interventricular septum (IVS thickness 13 mm, z-score +6) and LV posterior wall (LVPW thickness 15 mm, z-score +9.5) (**Figure 2B and 2C**), biventricular diastolic dysfunction and repolarization abnormalities. There were no ventricular arrhythmias. Family history was negative for sudden cardiac death or cardiomyopathies. Echocardiography revealed no abnormalities in both parents (aged 39 and 22 years) and the twin sister (aged 2 months).

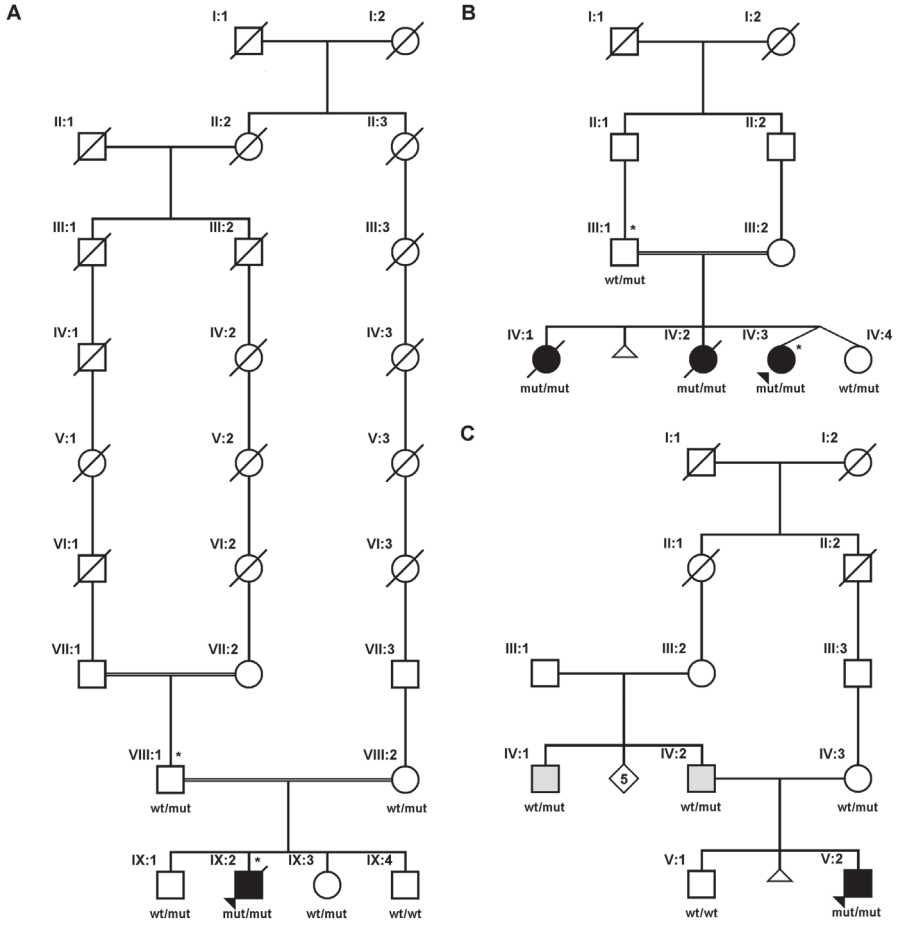

Figure 1. Pedigrees of families with *ALPK3*-related cardiomyopathy. Black-filled symbols represent severely affected individuals with homozygous mutations. Grey-filled symbols represent heterozygous individuals with adult-onset disease. Open symbols represent unaffected individuals. A diagonal line through the symbol indicates a deceased person. An arrowhead indicates the index patient. Individuals analyzed by exome sequencing are marked with an asterisk. *ALPK3* genotypes are shown below individuals: wt, wild-type allele; mut, mutant allele.

Family C. The index patient (C-V:2) is the second child of consanguineous Turkish parents. He was diagnosed with severe HCM at the age of 4 years. The disease was slowly progressive over the years. Out-of-hospital cardiac arrest occurred at age 7 due to ventricular arrhythmias, after which an implantable cardioverter defibrillator (ICD) was placed. Since then he has had several appropriate ICD shocks. Cardiac examination at age 11 years showed severe concentric LV hypertrophy (IVS 20 mm, z-score +11.2; LVPW 19 mm, z-score +13.1) without LV outflow tract obstruction (**Figure 2D and 2E**), moderate hypertrophy of the right ventricle (RV) and repolarization abnormalities. His father (C-IV:2) was diagnosed with HCM at the age of 27 years. Cardiac MRI at age 37 years showed concentric LV hypertrophy, most pronounced in the septum (IVS 32 mm) with relative sparing of the basal segments, and RV hypertrophy

(**Figure 2F**). Echocardiographic screening in the mother (aged 42 years) and older brother (aged 19 years) revealed no abnormalities. A paternal uncle (C-IV:1) had been diagnosed with HCM at the age of 29 years. Cardiac examination at age 45 years showed asymmetric septal hypertrophy (IVS 17 mm; LVPW 11 mm) and RV hypertrophy (7-8 mm, normal cut-off 5 mm).

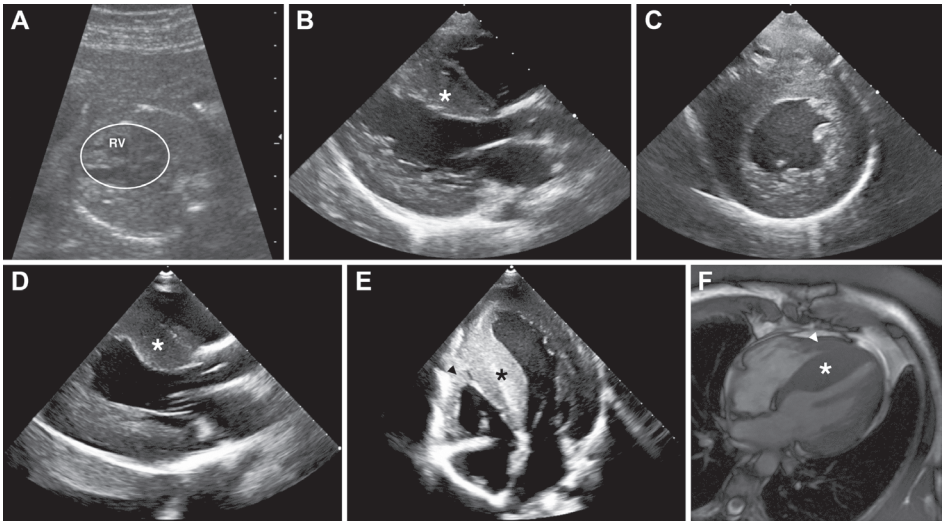

Figure 2. Cardiac imaging in *ALPK3*-related cardiomyopathy. Asterisk indicates the interventricular septum. Arrowhead indicates RV hypertrophy. (A) Prenatal ultrasound performed in patient B-IV:2 at 20 weeks of gestation showing an enlarged heart (encircled) with RV hypertrophy. Echocardiographic images: parasternal long axis (B) and short axis (C) views in patient B-IV:3 showing severe concentric LV hypertrophy. Parasternal long axis (D) and four chamber (E) views in patient C-V:2 showing severe concentric LV hypertrophy and moderate RV hypertrophy. (F) Cardiac MR image in patient C-IV:2 showing atypical distribution of LV hypertrophy with relative sparing of the basal segments, and RV hypertrophy.

Homozygosity mapping

In family A, we identified two chromosomal regions that were homozygous in the affected boy (IX:2) and heterozygous in his parents (VIII:1 and VIII:2) and unaffected brother (IX:1): 15q25.2q25.3 (84,058,592-89,164,874) and 21q21.3q22.11 (29,440,969-35,838,907). In family B, we identified three homozygous chromosomal regions shared by all affected individuals (IV:1, IV:2 and IV:3), whereas the unaffected father (III:1) and sister (IV:4) were heterozygous: 5q14.3q15 (90,263,863- 95,782,290), 15q25.1q25.3 (79,333,228- 87,165,178) and 16q23.2q24.3 (81,602,681- 90,148,796) (NCBI Build GRCh37/hg19). A small region (3.1 Mb) of homozygosity on chromosome region 15q25 overlapped between the affected individuals from both families.

Exome variant filtering

Exome sequencing was performed to target all exons and exon-intron junction sequences of known genes in the human genome for potential disease-causing variants. Using the above

described filtering pipeline, affected individuals from family A and B were found to harbor a homozygous variant in the alpha-kinase 3 (*ALPK3*) gene (**Supplemental Table 2**) located in the overlapping region of homozygosity on chromosome 15q25. Patient A-IX:2 was found to carry a homozygous intronic variant in the consensus acceptor splice site sequence of exon 10 of the *ALPK3* gene (c.4736-1G>A) (**Figure 3**), and this result was validated using Sanger sequencing. Both parents and two unaffected siblings (A-IX:1 and IX:3) were heterozygous for the mutation. One unaffected sibling (A-IX:4) carried the normal genotype. Patient B-IV:3 harbored a homozygous variant in exon 6 of the *ALPK3* gene introducing a premature stop codon (c.3781C>T, p.Arg1261*) (**Figure 3**). Sanger sequencing proved that all affected children were homozygous for this mutation. The father and unaffected sibling (B-IV:4) were heterozygous for the mutation. The mother was unavailable for testing, but is presumed to be a heterozygous carrier of the mutation as well.

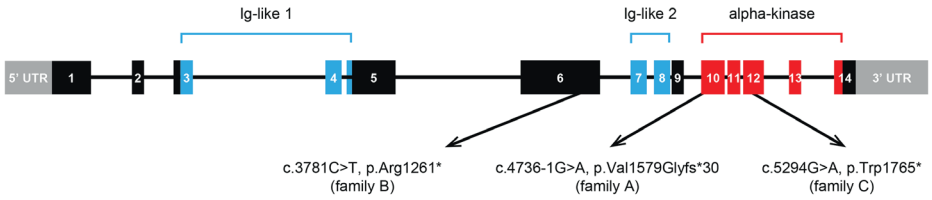

Figure 3. Schematic representation of the *ALPK3* gene. Boxes represent exons and untranslated regions (UTRs); connecting lines represent intervening introns. The three main functional domains, i.e. two immunoglobulin-like domains (in blue) and one alpha-type protein kinase domain (in red), and the positions of identified *ALPK3* mutations are indicated.

ALPK3 mutational screening

Subsequent Sanger sequencing of all coding regions and flanking intronic sequences of the *ALPK3* gene in a cohort of 60 unrelated patients with childhood-onset HCM or DCM uncovered the homozygous nucleotide substitution c.5294G>A in exon 12 introducing a premature stop codon (p.Trp1765*) in a third patient (family C) (**Figure 1C** and **Table 1**). His affected father and paternal uncle were shown to be heterozygous carriers; no additional mutation in the known cardiomyopathy genes was found (Detailed Methods, **Supplemental Information**). In the remaining cohort, no additional mutations in *ALPK3* were identified. Further studies will be performed in these patients to discover novel disease genes.

Splice variant analysis

The c.4736-1G>A variant in intron 9 (family A) was predicted to impair the natural acceptor splice site recognition using *in silico* tools. Sanger sequencing of cDNA from cultured fibroblasts of patient A-IX:2 confirmed skipping of exon 10, leading to a deletion of 281 nucleotides (**Supplemental Figure 1**). At the protein level, a frameshift starting at codon Val1579 and ending in a stop codon 29 positions downstream (p.Val1579Glyfs*30) is predicted.

Histology

Post-mortem macroscopic examination of the heart of individual A-IX:2 revealed severe cardiomegaly (total weight 34 g; normal 13.7 g) and biventricular dilatation. Microscopic examination of the myocardium showed subendocardial fibroelastosis without fatty replacement in both ventricles, fragmented elastin fibers and myxoid degeneration of the stroma (**Figure 4A**). Post-mortem macroscopic examination of the heart of individual B-IV:2 revealed severe cardiomegaly (total weight 34.7 g; normal 15.5 g) and biventricular dilatation with a large adherent thrombus to the left ventricle. Microscopic examination showed focal hypertrophy of the cardiomyocytes and extensive fibroelastosis in the subendocardial region without fatty infiltration (**Figure 4B and 4C**). No apparent myocyte disarray was observed both on evaluation with hematoxylin and eosin staining, and immunohistochemical staining for desmin (**Figure 4D**). Intercalated discs were difficult to recognize in both the patients and age-matched controls. Muscle biopsies from individual B-IV:3 (affected) and B-IV:4 (unaffected carrier) did not show any changes at routine histological and enzyme histochemical evaluation, including acid phosphatase, NADH-tetrazolium reductase, succinate dehydrogenase and cytochrome C oxidase.

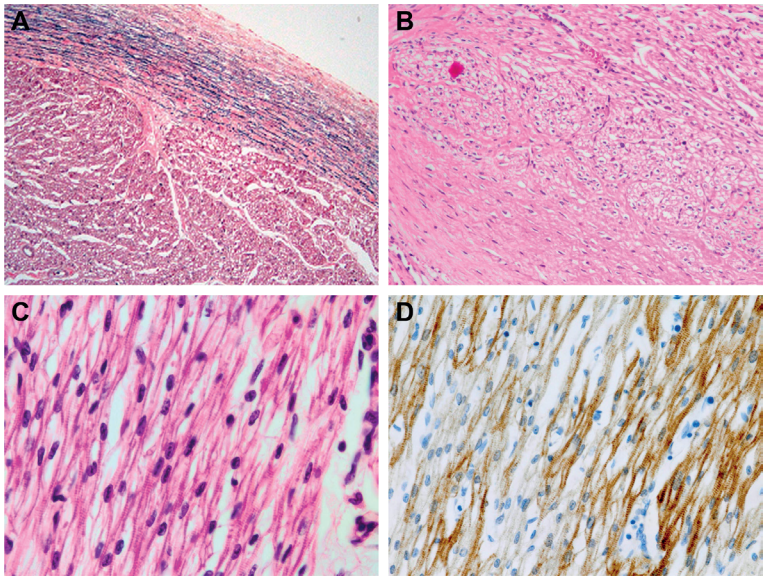

Figure 4. Histopathological examination of heart tissue in *ALPK3*-related cardiomyopathy. (A) Verhoeff-van Gieson staining for elastin at 20x magnification showing subendocardial fibroelastosis in patient A-IX:2. Hematoxylin and eosin (H&E) staining at 100x (B) and 630x magnification (C) showing focal hypertrophy of cardiomyocytes and subendocardial fibroelastosis without fatty infiltration in patient B-IV:2. Desmin staining (D) showing no apparent myocyte disarray. Intercalated discs were difficult to recognize in this patient (B-IV:2) and age-matched controls (data not shown).

Immunohistochemistry

To determine the effects of *ALPK3* mutations at the level of the intercalated discs, we performed immunohistochemical analysis of junctional proteins in cardiac tissue from one patient (A-IX:2) and two age-matched controls. Immunoreactive signal levels for the desmosomal proteins plakoglobin and desmoplakin were absent at intercalated discs in the patient sample. Signal levels for the other desmosomal protein plakophilin-2, the adhesion molecule N-cadherin, and the gap-junction protein connexin-43 were normal when compared to controls (**Figure 5**). Results of desmin staining were inconclusive (data not shown), as intercalated discs were difficult to recognize in both the patient and control samples.

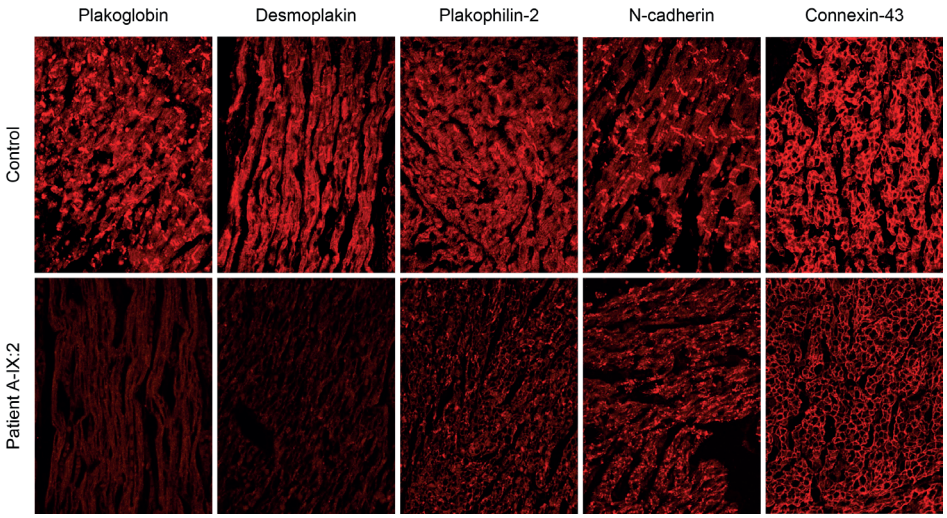

Figure 5. Immunofluorescence images of myocardial tissue from patient A-IX:2 and an unaffected control. Immunoreactive signals for plakoglobin and desmoplakin are absent at intercalated discs in the patient sample, whereas signal levels for plakophilin-2, N-cadherin and connexin-43 are normal when compared to the control samples.

Discussion

We identified a novel gene, *ALPK3*, involved in human cardiomyopathy. Biallelic truncating *ALPK3* mutations were identified in five patients with diverse ethnic backgrounds who presented with severe, early-onset cardiomyopathy. Four patients were diagnosed during fetal life or within the first hours after birth. The fifth patient was asymptomatic until the age of 4 years. Three out of five patients died due to progressive heart failure between 35 weeks of gestation and five days after birth. The patients who died exhibited features of DCM, or a combination of DCM and HCM. Two patients who were still alive at the age of 11 years showed severe concentric HCM. Although classic HCM and DCM primarily affect the left ventricle, three patients also displayed significant RV involvement. Interestingly, two heterozygous family members (C-IV:1 and IV:2) were diagnosed with an atypical form of HCM at young adult

age. Cardiac examination of the other proven and obligate heterozygotes (n=8, age range: 2 months to 42 years) did not reveal any evidence of cardiomyopathy. Although these numbers are limited, one may surmise that *ALPK3* mutation carriers have an increased risk of developing cardiomyopathy and therefore periodic screening should be considered.

The *ALPK3* gene is the human ortholog of the murine *Myocytic induction/differentiation originator* (also known as *Midori*). In 2001, the *Alpk3* gene was identified by applying a differential display technique in the P19CL6 cell line, which can be differentiated into beating cardiomyocytes upon incubation with dimethyl sulfoxide. Overexpression of *Alpk3* promoted their differentiation into cardiomyocytes, whereas differentiation was inhibited by blockade of *Alpk3* expression [18]. The gene has been mapped to chromosome 15q25.2 and contains 14 exons (**Figure 3**). The ALPK3 protein contains two immunoglobulin (Ig)-like domains and an alpha-type protein kinase domain. All three private homozygous mutations identified in this study are predicted to create premature stop codons, leading to nonsense mediated decay or truncated proteins with partial or complete removal of the kinase domain (**Figure 3**). We therefore hypothesize that these mutations result in loss of function of ALPK3. Alpha-kinase 3 belongs to a family of atypical protein kinases that recognize phosphorylation sites in the context of alpha-helices. Alpha-kinases are known to regulate a wide range of cellular processes, including cell migration, adhesion and proliferation, protein translation, vesicular transport and magnesium homeostasis [19, 20].

In mouse embryos, expression of *Alpk3* was restricted to fetal and adult hearts and adult skeletal muscle. Interestingly, *Alpk3* knock-out mice display cardiomyopathy with striking similarities to the human phenotype described here [21]. Although concentric cardiac hypertrophy of both the left and right ventricle was the predominant feature in *Alpk3*-deficient mice, other changes typically associated with DCM were also observed such as increased end-diastolic and end-systolic LV volume and a reduction in cardiac outflow, stroke volume, and ejection fraction [21]. Detailed histological and ultrastructural analysis of hearts from *Alpk3* -/- mice showed markedly reduced numbers of indistinct and fragmented intercalated discs and diffuse mild myofibrillar disarray, resulting in looser arrangement of adjacent myofibrils [21]. Interstitial fibrosis, one of the pathological hallmarks of cardiomyopathies, was absent. In contrast to the observations in *Alpk3* knockout mice, we observed extensive fibroelastosis without apparent myocyte disarray in our human cardiac samples (**Figure 4**).

Intercalated discs play an essential role in the mechanical and electrochemical coupling between adjacent cardiomyocytes. There are three main junctional complexes within the disc: fascia adherens, desmosomes and gap junctions. At an early age, intercalated discs are difficult to visualize under light microscopy, as exemplified in this study. Unfortunately, no patient material was available for ultrastructural examination using electron microscopy. However,

immunohistochemical analysis in myocardial tissue from one patient revealed the absence of desmosomal proteins plakoglobin and desmoplakin signals at the intercalated discs, whereas signals for the other junctional proteins were normal (**Figure 5**). Reduced immunoreactive signals for plakoglobin at cell-cell junctions have been observed in the majority of patients with ARVC. The specificity of this finding, however, is still under debate [17, 22]. Redistribution of plakoglobin from intercellular junctions to the intracellular space is believed to suppress canonical Wnt/beta-catenin signaling, leading to enhanced fibrogenesis and myocyte apoptosis [23]. Reduced signal levels for desmoplakin at intercalated discs, on the other hand, have mainly been demonstrated in patients with end-stage DCM due to mutations in the gene encoding desmin [24]. Altogether, our findings support a role for *ALPK3* in the formation and maintenance of intercalated discs. However, further studies in a larger cohort of patients are necessary to validate these findings.

The molecular mechanisms involved in the earliest stages of cardiac development are still largely unknown. *ALPK3* is expressed from the very early stage of cardiogenesis, prior to key transcription factors such as the NK-2 class homeobox transcription factor *NKX2-5*, the GATA-binding protein *GATA4* and the MADS-box transcription enhancer factor *MEF2C* [18]. Some cardiac transcription factors (e.g. HEY and HAND proteins) contain a helix-loop-helix domain, characterized by two alpha helices separated by a flexible loop structure, and might therefore be targets of ALPK3. By regulating the expression of these transcription factors, ALPK3 might control initial induction of differentiation and maturation of cardiomyocytes. Mutations in these putative downstream targets of ALPK3 have previously been associated with various congenital heart malformations and arrhythmias in humans [25]. Structural heart abnormalities were not observed in the patients described in this study. In recent years, however, some of these genes have also been implicated in familial forms of cardiomyopathy, including *NKX2-5*, *GATA4*, *GATA6* and the T-box transcription factors *TBX5* and *TBX20* [26-30]. Interestingly, mice lacking Xin actin-binding repeat-containing protein 1(*Xirp1*), a downstream target of *Nkx2-5* and *Mef2c*, display intercalated discs abnormalities and cardiac hypertrophy with conduction defects [31]. Further research into the transcription factor pathways involved in heart development and the putative role of ALPK3 in the related processes will provide more insight into the molecular pathways involved in pediatric cardiomyopathy and may have implications for the development of new therapeutic strategies.

Conclusions

We have shown that biallelic truncating mutations in *ALPK3* lead to severe pediatric cardiomyopathy in humans. Carriers may develop cardiomyopathy at adult age. *ALPK3*-related cardiomyopathy has morphological features of both HCM and DCM, and is characterized by

biventricular involvement and atypical distribution of hypertrophy. Our findings emphasize the essential role of cardiac transcription factor pathways in normal myocardial development. Further studies are necessary to understand how dysregulation of the transcriptional regulatory network results in cardiomyopathy.

Acknowledgements

We are grateful to the families for participating in this study. We would like to thank Kate Mc Intyre for editing this manuscript, and Tom de Vries Lentsch and René Frowijn for photographic artwork.

References

1. Lipshultz SE, Sleeper LA, Towbin JA et al. The incidence of pediatric cardiomyopathy in two regions of the United States. N Engl J Med 2003;348:1647-55.
2. Daubeney PE, Nugent AW, Chondros P et al. Clinical features and outcomes of childhood dilated cardiomyopathy: results from a national population-based study. Circulation 2006;114:2671-8.
3. Towbin JA, Lowe AM, Colan SD et al. Incidence, causes, and outcomes of dilated cardiomyopathy in children. Jama 2006;296:1867-76.
4. Elliott P, Andersson B, Arbustini E et al. Classification of the cardiomyopathies: a position statement from the European Society Of Cardiology Working Group on Myocardial and Pericardial Diseases. Eur Heart J 2008;29:270-6.
5. Kindel SJ, Miller EM, Gupta R et al. Pediatric cardiomyopathy: importance of genetic and metabolic evaluation. J Card Fail 2012;18:396-403.
6. Tariq M, Ware SM. Importance of genetic evaluation and testing in pediatric cardiomyopathy. World J Cardiol 2014;6:1156-65.
7. Seelow D, Schuelke M. HomozygosityMapper2012--bridging the gap between homozygosity mapping and deep sequencing. Nucleic Acids Res 2012;40:W516-20.
8. Li H, Durbin R. Fast and accurate long-read alignment with Burrows-Wheeler transform. Bioinformatics 2010;26:589-95.
9. Li H, Handsaker B, Wysoker A et al. The Sequence Alignment/Map format and SAMtools. Bioinformatics 2009;25:2078-9.
10. McKenna A, Hanna M, Banks E et al. The Genome Analysis Toolkit: a MapReduce framework for analyzing next-generation DNA sequencing data. Genome Res 2010;20:1297-303.
11. Boomsma DI, Wijmenga C, Slagboom EP et al. The Genome of the Netherlands: design, and project goals. Eur J Hum Genet 2014;22:221-7.
12. Consortium GP, Abecasis GR, Auton A et al. An integrated map of genetic variation from 1,092 human genomes. Nature 2012;491:56-65.
13. den Dunnen JT, Antonarakis SE. Mutation nomenclature extensions and suggestions to describe complex mutations: a discussion. Hum Mutat 2000;15:7-12.
14. Ng PC, Henikoff S. Predicting deleterious amino acid substitutions. Genome Res 2001;11:863-74.
15. Adzhubei IA, Schmidt S, Peshkin L et al. A method and server for predicting damaging missense mutations. Nat Methods 2010;7:248-9.
16. Schwarz JM, Cooper DN, Schuelke M, Seelow D. MutationTaster2: mutation prediction for the deep-sequencing age. Nat Methods 2014;11:361-2.
17. Asimaki A, Tandri H, Huang H et al. A new diagnostic test for arrhythmogenic right ventricular cardiomyopathy. N Engl J Med 2009;360:1075-84.
18. Hosoda T, Monzen K, Hiroi Y et al. A novel myocyte-specific gene Midori promotes the differentiation of P19CL6 cells into cardiomyocytes. J Biol Chem 2001;276:35978-89.
19. Middelbeek J, Clark K, Venselaar H, Huynen MA, van Leeuwen FN. The alpha-kinase family: an exceptional branch on the protein kinase tree. Cell Mol Life Sci 2010;67:875-90.
20. Drennan D, Ryazanov AG. Alpha-kinases: analysis of the family and comparison with conventional protein kinases. Prog Biophys Mol Biol 2004;85:1-32.
21. Van Sligtenhorst I, Ding ZM, Shi ZZ, Read RW, Hansen G, Vogel P. Cardiomyopathy in alpha-kinase 3 (ALPK3)-deficient mice. Vet Pathol 2012;49:131-41.
22. Munkholm J, Christensen AH, Svendsen JH, Andersen CB. Usefulness of immunostaining for plakoglobin as a diagnostic marker of arrhythmogenic right ventricular cardiomyopathy. Am J Cardiol 2012;109:272-5.
23. Garcia-Gras E, Lombardi R, Giocondo MJ et al. Suppression of canonical Wnt/beta-catenin signaling by nuclear plakoglobin recapitulates phenotype of arrhythmogenic right ventricular cardiomyopathy. J Clin Invest 2006;116:2012-21.

24. Otten E, Asimaki A, Maass A et al. Desmin mutations as a cause of right ventricular heart failure affect the intercalated disks. Heart Rhythm 2010;7:1058-64.
25. McCulley DJ, Black BL. Transcription factor pathways and congenital heart disease. Curr Top Dev Biol 2012;100:253-77.
26. Pashmforoush M, Lu JT, Chen H et al. Nkx2-5 pathways and congenital heart disease; loss of ventricular myocyte lineage specification leads to progressive cardiomyopathy and complete heart block. Cell 2004; 117:373-86.
27. Li RG, Li L, Qiu XB et al. GATA4 loss-of-function mutation underlies familial dilated cardiomyopathy. Biochem Biophys Res Commun 2013;439:591-6.
28. Xu L, Zhao L, Yuan F et al. GATA6 loss-of-function mutations contribute to familial dilated cardiomyopathy. Int J Mol Med 2014;34:1315-22.
29. Zhang XL, Qiu XB, Yuan F et al. TBX5 loss-of-function mutation contributes to familial dilated cardiomyopathy. Biochem Biophys Res Commun 2015;459:166-71.
30. Kirk EP, Sunde M, Costa MW et al. Mutations in cardiac T-box factor gene TBX20 are associated with diverse cardiac pathologies, including defects of septation and valvulogenesis and cardiomyopathy. Am J Hum Genet 2007;81:280-91.
31. Gustafson-Wagner EA, Sinn HW, Chen YL et al. Loss of mXinalpha, an intercalated disk protein, results in cardiac hypertrophy and cardiomyopathy with conduction defects. Am J Physiol Heart Circ Physiol 2007; 293:H2680-92.

Supplemental Information

Detailed Methods

Patient A-IX:2. Biochemical studies, including analysis of blood glucose, lactate, pyruvate, creatine kinase, amino acids, acylcarnitines, and sialotransferrin levels were normal. Total and free carnitine levels were extremely elevated due to supplementation and massive cellular tissue death. Enzyme studies in fibroblasts showed normal carnitine palmitoyltransferase I and II, α and β-glucosidase, and β-galactosidase activities. Monolysocardiolipin/cardiolipin ratio was normal. Viral serology showed no abnormalities. Sanger sequencing of the genes *DES* (NM_001927.3), *LMNA* (NM_001257374.2), *MYBPC3* (NM_000256.3), *MYH7* (NM_000257.3), *MYL2* (exon 7, NM_000432.3), *TAZ* (NM_181312.3), *TNNI3* (NM_000363.4) and *TNNT2* (NM_001001430.2) revealed no abnormalities.

Patient B-IV:1. Conventional karyotyping results of amniotic fluid cells were normal (46,XX). Serological testing for intrauterine infections showed elevated IgM antibodies for herpes simplex virus (HSV). Postmortem nasal and throat swabs were negative for HSV.

Patient B-IV:2. Conventional karyotyping results were normal (46,XX). Microbiological studies, including PCR, serology and blood and ascites cultures, were negative. Extensive metabolic screening, including analysis of blood glucose, lactate, amino acids, organic acids, total and free carnitine, acylcarnitines and very long-chain fatty acids levels revealed no evidence of an inborn error of metabolism. Isoelectric focusing of serum transferrin was normal. Enzyme studies in fibroblasts showed normal hexosaminidase A and B, β-galactosidase, α and β-glucosidase, β-glucuronidase, galactose-6-sulfatase, galactosyl ceramidase, iduronate 2-sulfatase, α-iduronidase, sfingomyelinase, neuraminidase and phosphomannomutase activities. Mutation analysis of common mitochondrial DNA point mutations (A3243G, A8344G, T8933G/C, A3260G, A4300G, A4269G and A4317G) and deletions revealed no abnormalities.

Patient B-IV:3. Extensive metabolic screening, including analysis of blood glucose, lactate, pyruvate, amino acids, organic acids, total and free carnitine, acylcarnitines, oligosaccharides, sialic acids, and very long-chain fatty acids levels revealed no evidence of an inborn error of metabolism. Isoelectric focusing of serum transferrin was normal. Enzyme activity studies of the individual complexes of the respiratory chain showed no abnormalities. Next-generation sequencing (paired-end 150 bp, Miseq, Illumina) of 46 cardiomyopathy-related genes showed a homozygous variant, c.393-5C>A, in the *SCN5A* gene (NM_000335.4). This variant has been reported in heterozygous state in a patient with long QT syndrome and has been found at a low frequency in several populations (rs368678204) [1]. However, this variant was also present in 3 out of 93 Moroccan control samples. In addition, RT-PCR analysis showed that this variant does not affect splicing (data not shown). The variant was therefore classified as "likely benign"

(class 2). Analysis of the other 45 genes, *ABCC9* (NM_020297.2), *ACTC1* (NM_005159.4), *ACTN2* (NM_001103.2), *ANKRD1* (NM_014391.2), *BAG3* (NM_004281.3), *CALR3* (NM_145046.3), *CASQ2* (NM_001232.2), *CAV3* (NM_033337.2), *CRYAB* (NM_001885.1), *CSRP3* (NM_003476.3), *DES* (NM_001927.3), *EMD* (NM_000117.2), *FHL1* (NM_001159702.2), *FKTN* (NM_001079802.1), *GLA* (NM_000169.2), *ILK* (NM_004517.2), *JPH2* (NM_020433.4), *LAMA4* (NM_001105206.1), *LAMP2* (NM_002294.2), *LDB3* (NM_007078.2), *LMNA* (NM_170707.2), *MYBPC3* (NM_000256.3), *MYH7* (NM_000257.2), *MYL2* (NM_000432.3), *MYL3* (NM_000258.2), *MYOZ2* (NM_016599.3), *MYPN* (NM_032578.2), *NEXN* (NM_144573.3), *NRG1* (NM_013956.3), *PDLIM3* (NM_014476.4), *PLN* (NM_002667.3), *PRKAG2* (NM_016203.3), *RBM20* (NM_001134363.1), *SGCD* (NM_000337.5), *TAZ* (NM_000116.3), *TBX20* (NM_001077653.2), *TCAP* (NM_003673.3), *TMPO* (NM_003276.2), *TNNC1* (NM_003280.2), *TNNI3* (NM_000363.4), *TNNT2* (NM_001001430), *TPM1* (NM_001018005.1), *TTN* (NM_003319.4), *TTR* (NM_000371.3) and *VCL* (NM_014000.2) revealed no abnormalities.

Patient C-IV:2. Sanger sequencing of the genes *ACTC1* (NM_005159), *CSRP3* (NM_003476.2), *MYBPC3* (NM_000256), *MYH7* (NM_000257), *MYL2* (NM_000432), *TCAP* (NM_003673.2), *TNNI3* (NM_000363), *TNNT2* (NM001001430.1) and *TPM1* (NM_000366; NM_001018005) revealed no abnormalities. Next-generation sequencing (paired-end 150 bp, Miseq, Illumina) of 48 cardiomyopathy-related genes showed two heterozygous missense variants, c.61922G>A (p.Arg20641Gln) and c.98294C>G (p.Ala32765Gly), in the *TTN* gene (NM_001267550.1). These variants have been found at a low frequency in various populations (rs199895260 and rs72648273, respectively) and were classified as "variant of unknown significance" (class 3). Analysis of the other 47 genes, *ABCC9* (NM_020297.2; NM_020298.2), *ACTC1* (NM_005159.4), *ACTN2* (NM_001103.2), *ANKRD1* (NM_014391.2), *BAG3* (NM_004281.3), *CALR3* (NM_145046.3), *CAV3* (NM_033337.3), *CRYAB* (NM_001885.1), *CSRP3* (NM_003476.3), *CTNNA3* (NM_013266.2), *DES* (NM_001927.3), *DSC2* (NM_024422.3; NM_004949.3), *DSG2* (NM_001943.3), *DSP* (NM_004415.2), *EMD* (NM_000117.2), *FHL1* (NM_001159699.1; NM_001159701.1; NM_001159702.2;), *GLA* (NM_000169.2), *JPH2* (NM_020433.4; NM_175913.3), *JUP* (NM_021991.2), *LAMA4* (NM_001105206.1; NM_001105208.1), *LAMP2* (NM001122606.1; NM_002294.2; NM_013995.2), *LDB3* (NM_001080116.1; NM_007078.2), *LMNA* (NM_001257374.1; NM005572.3; NM170707.3), *MIB1* (NM_020774.2), *MYBPC3* (NM_000256.3), *MYH6* (NM_002471.3), *MYH7* (NM_000257.2), *MYL2* (NM_000432.3), *MYL3* (NM_000258.2), *MYOZ2* (NM_016599.3), *MYPN* (NM_032578.2), *NEXN* (NM_144573.3), *PKP2* (NM_004572.3), *PLN* (NM_002667.3), *PRDM16* (NM_22114.3), *PRKAG2* (NM_016203.3), *RBM20* (NM_001134363.1), *SCN5A* (NM_001160160.1; NM_198056.2), *TAZ* (NM_000116.3), *TCAP* (NM_003673.3), *TMEM43* (NM_024334.2), *TNNC1* (NM_003280.2), *TNNI3* (NM_000363.4), *TNNT2* (NM_000364.2; NM_001001430.1), *TPM1* (NM000366.5; NM_001018005.1; NM_001018020.1), *TTR* (NM_000371.3) and *VCL* (NM_014000.2) revealed no abnormalities. SNP array analysis (Infinium CytoSNP-850K BeadChip) showed a normal male pattern.

Patient C-V:2. Metabolic screening, including analysis of amino acids, organic acids, sialic acids, total and free carnitine, acylcarnitines, oligosaccharides and mucopolysaccharides levels revealed no evidence of an inborn error of metabolism. SNP array analysis (Affymetrix GeneChip Human Mapping 250K Nsp) showed several large regions of homozygosity, consistent with known parental consanguinity.

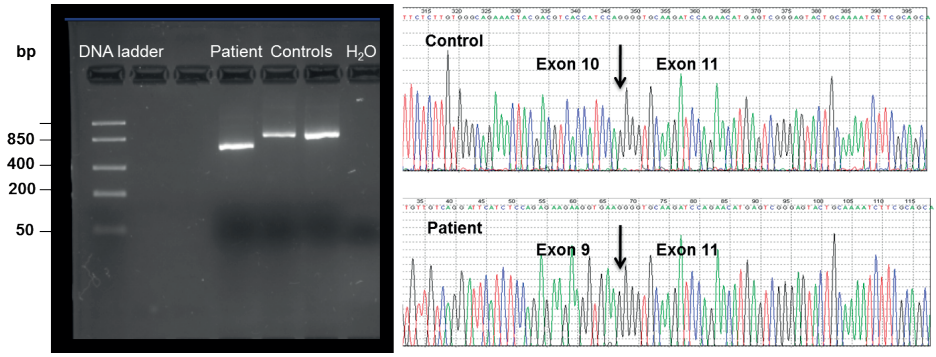

Supplemental Figure 1. Results of reverse transcriptase PCR analysis. To investigate the effect of the *ALPK3* c.4736-1G>A variant on RNA splicing, we designed a reverse transcriptase PCR experiment (RT-PCR) using RNA isolated from fibroblasts of patient A-IX:2 (cDNA forward primer sequence 5′-GTGCACCATCCACAATGAGC-3′, cDNA reverse primer sequence 5′-GACTAGGGAGGCCTTTCTTCTG-3′). Low range DNA ladder is used as size standard. Analysis of the resulting RT-PCR product, covering *ALPK3* exon 10 and flanking sequences in the wild-type situation, by 2% agarose gel electrophoresis showed a smaller product in the patient (± 630 nucleotides) compared to the controls (± 900 nucleotides). Subsequent Sanger sequencing of the respective RT-PCR products confirmed that the *ALPK3* c.4736-1G>A mutation leads to complete skipping of exon 10, which consists of 281 nucleotides.

Supplemental Table 1. Primer sequences used for Sanger sequencing

Name	Forward primer	Reverse primer	Amplicon size
ALPK3_ex1A	5′-GAAGTGTTAATTGAGCCCCTAATCT-3′	5′-CGCGCCCCTATTTATAGCC-3′	437
ALPK3_ex1B	5′-GCGCTACTGCAGACACCAG-3′	5′-ccctcacagggactgatcc-3′	498
ALPK3_ex2	5′-atggagcaggccaactaagac-3′	5′-gttagtgcacgagcagacactc-3′	279
ALPK3_ex3	5′-caggcatggtaagacggaag-3′	5′-gtcacctcacgtagttttgtgc-3′	335
ALPK3_ex4	5′-gcctcttcccattattttgga-3′	5′-cagactgctccatttctgagg-3′	264
ALPK3_ex5A	5′-gttgtatgttgtgacgtgtgagatg-3′	5′-CAGAAGCAAAACTGTTGATCAGG-3′	549
ALPK3_ex5B	5′-ACCATGACTGAGTACAAGATCCAC-3′	5′-GCTGGCTTCCTGGTACTATCTGT-3′	659
ALPK3_ex5C	5′-GCCTGACTCCTGTGGGACT-3′	5′-tgcagcaagagtttccatga-3′	668
ALPK3_ex6A	5′-ggatgccagactggaaagag-3′	5′-TGGTTCCTGGAGGCTGTTAC-3′	774
ALPK3_ex6B	5′-ACACAGGAAGACAGAAGGATGC-3′	5′-CCAGTTCCAGGAAGAGAAGG-3′	548
ALPK3_ex6C	5′-GTATGGATCAGGGTGGCTGT-3′	5′-AGGGACAGTGAGGGAGCTG-3′	671
ALPK3_ex6D	5′-CTGCTGAGCCCCTGTACCT-3′	5′-CTGCTCTGACCTTAGGGAGAAAT-3′	433
ALPK3_ex6E	5′-CCCTCCCAAGAGGAGAAGTT-3′	5′-gttagcagcagcagcagtgt-3′	483
ALPK3_ex7	5′-gcttctctctagctgagatgtgtg-3′	5′-gaataaaaGgacctcccctggt-3′	485
ALPK3_ex8	5′-aggactgcaaaccagacctgt-3′	5′-gccttctctcaaagatgaCtgc-3′	387
ALPK3_ex9	5′-ggcagcagtcatctttgagag-3′	5′-aagggtgaactaactcctgtgc-3′	338
ALPK3_ex10	5′-ccttttccttccctgtgagc-3′	5′-tactgggcatcctaacaggac-3′	444
ALPK3_ex11	5′-agtcccctaacagaataggtagcc-3′	5′-attttgtgaggccactgagc-3′	343
ALPK3_ex12	5′-ggcccttctttttaggtccaag-3′	5′-cactatggctttgcctcctc-3′	395
ALPK3_ex13	5′-gcaggaagagacatggttctaagc-3′	5′-gcatcagtaatagctgccacac-3′	360
ALPK3_ex14	5′-atgtaccctgagcacgacatc-3′	5′-GCACCTTCTCCAGTTAGTTCCA-3′	555

Supplemental Table 2. Whole exome sequence variant filtering

Filtering step	Family A	Family B
Input variants	32802	38784
Read depth ≥6	31931	38261
Exons and flanking sequences	28040	28985
Population frequency	2463	2269
Heterozygous in father	1268	893
Homozygous in patient	60	133
Effect on protein	37	107
Presence in homozygous regions	1	8
Overlapping genes		1

Supplemental References

1. Hedley PL, Jorgensen P, Schlamowitz S et al. The genetic basis of long QT and short QT syndromes: a mutation update. Hum Mutat 2009;30:1486-511.